mathematics

MDPI

Article

An Analysis of Climate Change Based on Machine Learning and an Endoreversible Model

Sebastián Vázquez-Ramírez [1], Miguel Torres-Ruiz [1,*], Rolando Quintero [1], Kwok Tai Chui [2] and Carlos Guzmán Sánchez-Mejorada [1]

1 Instituto Politécnico Nacional, CIC, UPALM-Zacatenco, Mexico City 07320, Mexico; svazquezr1102@alumno.ipn.mx (S.V.-R.); rquintero@ipn.mx (R.Q.); cmejora@ipn.mx (C.G.S.-M.)
2 Department of Electronic Engineering and Computer Science, School of Science and Technology, Hong Kong Metropolitan University, Hong Kong, China; jktchui@hkmu.edu.hk
* Correspondence: mtorresru@ipn.mx; Tel.: +52-(55)-5729-6000 (ext. 56590)

Abstract: Several Sun models suggest a radioactive balance, where the concentration of greenhouse gases and the albedo effect are related to the Earth's surface temperature. There is a considerable increment in greenhouse gases due to anthropogenic activities. Climate change correlates with this alteration in the atmosphere and an increase in surface temperature. Efficient forecasting of climate change and its impacts could be helpful to respond to the threat of c.c. and develop sustainably. Many studies have predicted temperature changes in the coming years. The global community has to create a model that can realize good predictions to ensure the best way to deal with this warming. Thus, we propose a finite-time thermodynamic (FTT) approach in the current work. FTT can solve problems such as the faint young Sun paradox. In addition, we use different machine learning models to evaluate our method and compare the experimental prediction and results.

Keywords: clustering; machine learning; greenhouse gas; finite-time thermodynamics; climate change

MSC: 68U01

check for updates

Citation: Vázquez-Ramírez, S.; Torres-Ruiz, M.; Quintero, R.; Chui, K.T.; Guzmán Sánchez-Mejorada, C. An Analysis of Climate Change Based on Machine Learning and an Endoreversible Model. *Mathematics* **2023**, *11*, 3060. https://doi.org/10.3390/math11143060

Academic Editor: Wei Fang

Received: 15 June 2023
Revised: 8 July 2023
Accepted: 9 July 2023
Published: 11 July 2023

1. Introduction

The issue of climate change stands as one of the most significant obstacles that humanity must confront. Thus, extensive scientific evidence demonstrates that the altering climate has significantly impacted societies throughout history and in the present, posing severe effects for the future. Modern advancements in quantitative empirical studies have shed light on the crucial interconnections within the interconnected climate–human system [1]. Various statistical studies have explored the cause-and-effect relationship between particular climate conditions and their influence on social interaction, agriculture, economics, migratory flows, and health [2].

The emergence of scientific efforts in different fields has created a consensus concerning the sustainable development of initiatives and strategies to mitigate climate change. The most severe consequences of climate change directly affect the health of citizens due to human activities causing the proliferation of greenhouse gases in the atmosphere, which induces the increase in temperatures and alteration of the hydrologic cycle [3]. The analysis of the climate change situation is very timely, because secondary effects are associated with the negative impact on agriculture, the geographic distribution of infectious diseases, large-scale migrations, clean water access, and others [4].

Machine learning techniques have recently successfully employed statistical downscaling methods for global climate models. According to Nourani et al. [5], a diverse range of machine learning models have been developed and used in groundwater modeling and other prediction tasks within the field of environmental engineering [6]. Prediction models focused on machine learning to analyze climate variables such as precipitation and temperature have been proposed in other studies to improve accuracy [7]. The support vector regression model, the adaptive neurofuzzy inference system, and the feedforward neural network (FFNN) are the most frequently employed machine learning models to analyze climate change and particular groundwater levels [8,9]. Other approaches are based on Gaussian models, which are suitable methods for global climate modeling [10].

Recently, there has been a growing emergence of deep learning models that have garnered significant attention across various engineering disciplines due to their ability to extract features from data. Among these models, the long short-term memory (LSTM) neural network stands out as a powerful deep learning model capable of capturing sequential characteristics from time series data. LSTM has already been successfully applied in groundwater-level modeling, as demonstrated by Nourani et al. [11]. According to the literature review, decision trees, random forests, and artificial neural networks are the most commonly applied machine algorithms to analyze climate change risk assessment. They have enabled the identification, classification, and detection of targets and environmental and structural features, particularly flood and landslide risk events [12].

In the same context, analyzing changes in hydrological systems directly impacts global climate change, in which classic machine learning algorithms could be limited to quantifying events related to the climate variability in those hydrological systems. However, the Gaussian process regression method has been demonstrated to improve the analysis concerning nonlinear climate variables [13].

On the other hand, the literature reports a crucial synergy between the physics-based models and machine-learning techniques to develop hybrid approaches to climate change analysis [14]. Thus, Chukwujindu et al. [15] revealed a crucial relationship between physics and artificial intelligence to understand better the climate change caused by solar radiation.

According to the development and integration of multidisciplinary fields, the last years have involved applying physics theories to analyze various Earth phenomena. Now, physicists and computer scientists have demonstrated enormous interest in studying the aforementioned secondary effects of climate change. In this sense, Jusup et al. [16] considered "social physics" an essential tool to quantify social and environmental phenomena. Moreover, this approach is oriented toward analyzing different issues in which this discipline can explicitly explain each phenomenon. For instance, in addressing the climate change topic, the use of network area to describe the complex problem of Earth's climate system evidences how physics methods are suitable to work in a multidisciplinary way with other fields to face this issue quantitatively.

Addressing the risks associated with climate change, Steffen et al. [17] recognized the relationship between the social community and climate. Therefore, this strategy extends beyond solely understanding the physical aspects, and requires mobilizing human action. Scientists are striving to meet this challenge by integrating climate science, social sciences, computer science, and humanities, resulting in a new field called earth system science, which aims to foster a holistic understanding of the Earth's complex dynamics.

On the other hand, global warming is a visible consequence of the heightened intensity and frequency of extreme weather and climate events, which encompass a range of phenomena, including heatwaves, droughts, wildfires, floods, and hurricanes. These extreme events pose a substantial risk to human lives and livelihoods, evident through consequences such as fresh and clean water scarcity and diminished food production. Such extreme events are characterized by the climatic variable surpassing a critical threshold. It is worth noting that some extreme events may arise from natural climate variability and are not directly linked to human-induced forces [18].

There is a high degree of confidence that the anthropogenic rise in greenhouse gas concentrations and other human-induced factors is responsible for more than 50% of the reported global average surface temperature accumulation between 1951 and 2010 [16].

Thus, considering the theoretical foundations presented in [16,19], we propose a finite-time thermodynamic approach to model and predict Earth's global warming, comparing the results of the model with the implementation of machine learning techniques to assess the predictions.

Finite-time thermodynamics (FTT) has been developed by placing realistic limits on irreversible processes through various properties, such as power, efficiency, and dissipation. FTT can be considered an extension of classical equilibrium thermodynamics (CET), in which thermodynamic models more similar to the real world are sought compared to those given by CET. So, these models consider the irreversibilities of the system [20,21]. The approach incorporates the constraints of finite-time operation; constraints on system variables; and generic models for the sources of irreversibility, and thus the production of entropy such as finite rate, heat transfer, friction, and heat leakage, among others [22]. Moreover, an extreme or optimum of a thermodynamically significant variable is calculated, such as minimizing entropy production, maximizing energy or availability, and maximizing power and efficiency [22]. The pioneering work of the FTT corresponds to Curzon and Ahlborn [20,22], in which the fundamental limits of a power plant used a *machine endoreversible* model. This is made up of an endoreversible Carnot cycle, where the irreversible processes involve the exchange of heat between the thermal reservoirs and the active substance.

The thermal engine is composed of two temperature stores, T_1 and T_2, where $T_1 > T_2$, two irreversible components that are the two thermal resistances, which produce thermal flows towards the reversible Carnot engine with intermediate temperatures T_{1w} and T_{2w}, with $T_{1w} > T_{2w}$, placed between the intermediate stores. The model considers a linear heat transfer between two irreversible components (thermal conductances α and β) conductances (see Figure 1).

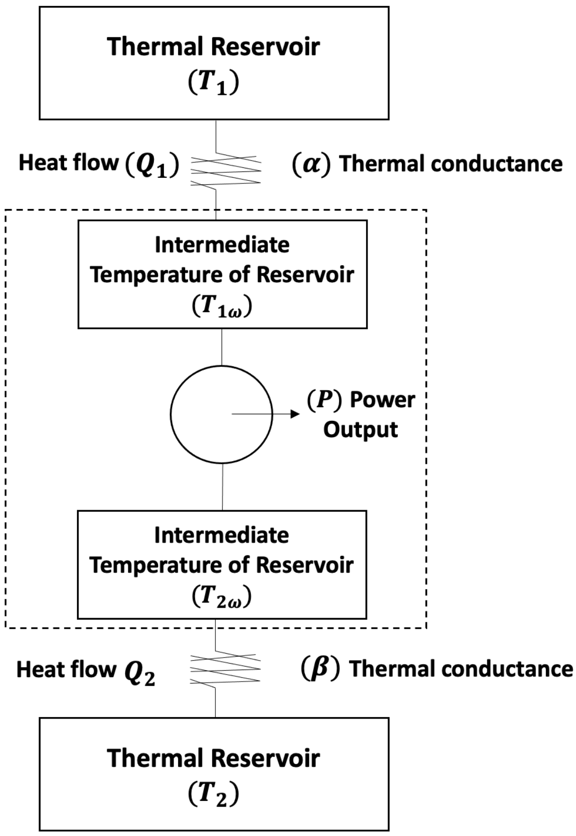

Figure 1. Scheme of a endoreversible model proposed by De Vos [23].

Summing up, Figure 1 shows a schematic representation of the endoreversible Curzon–Ahlborn engine. It is built by two reservoirs of temperatures T_1 and T_2, respectively: α and β, which denote thermal conductance constants, and a reversible Carnot engine represented by $T_{1\omega}$ and $T_{1\omega}$, where P is the power output of the cycle.

A problem solved by finite-time thermodynamics efficiently is the so-called weak young Sun paradox proposed by Sagan and Mullen [24]. This study presents a drawback for understanding the early stages of planet Earth, since the Sun's luminosity about 4.5 Gyr ago was between 70–80% of its value to operate [24–26]. So, it represents a terrestrial temperature below the water freezing point. The planet's surface temperature is controlled by the solar radiation it acquires and its interchange with the gases in the atmosphere. We consider a blackbody radiative equilibrium between the young Sun and the Earth obtained in a surface temperature T = 255K, low enough to keep most of the planet's surface frozen down to 1–2 Gyr [24]. However, several studies, together with sedimentary records, suggest the existence of an average surface temperature capable of having liquid water for almost the entire history of the planet [24]. So, to resolve such a paradox, the first assumption is taken that solar radiation has increased in the Sun's lifetime due to the increase in density of the solar nucleus [24]. The luminosity of the young Sun has been estimated to be 30% less than the actual value received from the Sun, according to what was said by Gough [24], where I_{sc} is the present luminosity of the Sun and $t_0 \approx 4.56$ Gyr, which is the present age of the Sun. Equation (1) shows the evolution of the Sun's luminosity, and this equation affects the amount of average solar radiation $\bar{q}_s = I_{sc}(1-\rho)/4$ received by the planet. The equation of the luminosity of Gough is expressed in the following way:

$$I(t) = \left[1 + 0.4\left(1 - \frac{t}{t_0}\right)\right]^{-1} I_{sc} \tag{1}$$

Based on the foundation, the problem of thermodynamic equilibrium between the solar system's planets depends on the influx of solar incident I_{sc}, the Earth's albedo ρ, and the effect of greenhouse γ. Thus, the issue of the thermal equilibrium among solar system planets and a correct temperature estimation is solved based on the atmosphere's physical characteristics. Curzon and Ahlborn [22] introduced the finite-time thermodynamics concept. They achieved this using a Carnot cycle model, incorporating limited heat transfer between the heat reservoir and the working substance, all within a maximum-power operating regime. Following its initial introduction, finite-time thermodynamics underwent further development to encompass various operating regimes, including—but not limited to—efficiency power, ecological function, and more. Using the FTT-based approach in creating models for power converters results in more accurate representations of their operational levels in real-world scenarios. In [20], an atmospheric convection model, known as the Gordon–Zarmi (GZ) model, was introduced to estimate the temperature of the Earth's lowest atmospheric layer and establish an upper limit for average wind power. The GZ model incorporates a convection cell, an endoreversible Carnot cycle, and two external thermal reservoirs, such as air, surrounding the active substance.

The study presented in [27] examined the endoreversible model and recognized that there is a dissipation of wind energy. The authors proposed to derive an upper limit for the efficiency of converting solar energy into wind energy, which is approximately 8.3%, assuming the atmospheric "heat engine" is fully powered by a complete power engine.

On the other hand, Van der Wel improved a new efficiency of the solar energy upper bound $w_{max} \approx 10.23\%$ with another endoreversible model based on convective Hadley cells [24,28]. The peculiarity of the GZ models is that they offer a potential resolution to the paradox known as the "young and weak Sun", which was initially introduced by Carl Sagan and George Mullen in 1972 [25,26]. The GZ and Gough models examine the evolution of the solar constant, enabling the investigation of potential future scenarios for Earth's temperature. These models employ various objective functions, including maximum power, efficient power, and ecological function, to analyze and assess these scenarios.

Hence, the present research study aims to investigate the planet's surface temperatures resulting from the escalating levels of greenhouse gases. The approach involves analyzing the thermodynamic behavior of the atmosphere within a finite-time regime. We decided to employ this methodology, considering the good results in predicting climate change in several geologic eras in the past. So, it is possible to modify and set the endoreversible machine model to forecast temperatures derived from climate change in the coming years.

The remaining paper is organized as follows: The subsequent section consists of comprehensive state-of-the-art climate change models based on different approaches. Section 3 describes the preliminary foundations concerning finite-time thermodynamics; Section 4 outlines the methods related to the proposed endoreversible model; and Section 5 describes the proposed model and its peculiarities. Section 6 shows the experimental results, and the discussion of the outcomes and findings are included in Section 7, and the last section involves the conclusion and future works.

2. Related Work

Global warming caused by human activities represents one of the most significant challenges of the present time. The classical approaches concerning climate change have studied complex systems such as differential equations and developments in chaos theory. Nevertheless, the large amount of data available allows us to use artificial intelligence techniques, which are more straightforward than those used by the areas of complexity science, resulting in the prediction of future scenarios due to climate change.

According to Houghton [29], global warming is a climate system where several variables are responsible for raising global average temperatures. Most of these effects are related to the radiative balance of the planetary atmosphere: water vapor feedback, cloud radiation feedback, and ocean circulation feedback. In consequence, all of them refer to the albedo and greenhouse effects. Therefore, to forecast global warming, a set of characteristics that affect the global emission of greenhouse gases must be taken. These gases have had a notable increase due to anthropogenic behavior and activity. Development projections of global average temperature changes for the present century are in the range of 0.15–0.6 °C per decade. Understanding this problem allows us to consider humans' and ecosystems' impacts and adaptive capacity [29].

One of the major consequences of global warming is the melting of ice bodies on the Earth. The Arctic Sea is one of the leading indicators of the increase in average temperature. The study of the ice concentration and the rise in sea level has various approaches, one of which that is widely used is deep learning techniques to predict how the ice concentration changes with the increase in average temperature [30]. In the same way that the Arctic layers and their melting show the effect of climate change, all oceans experience the same significant warming and a rising sea level, so it is necessary to generate diagnostic and prognostic prediction models to elucidate these increases and their risks, since they are associated with other adverse events such as the propagation of cycles, lack of rain, and the growth and spread of diseases. According to diverse authors, the combination of machine learning and deep learning techniques can give us entirely accurate predictions for the future [31–34].

In the study carried out by Sidhu et al. [35], the use of machine learning is analyzed to understand the impact of climate change on different types of crops, taking into account climate–yield relationships. The authors compared the usual linear regression technique for estimating historical data to approximate yield against climate change and using boosted regression trees. The conclusions suggested that interpreting results based on a single model can generate biases in the information obtained.

On the other hand, due to the high economic and social impacts associated with climate change, it is essential to understand the causes and identify the patterns of the obtained data to make correct predictions. According to Zheng et al. [36], the construction of a reliable model based on experimental data and the relationship between temperature and the concentration of gases in the atmosphere such as carbon dioxide (CO_2), nitrous oxide (N_2O) and methane (CH_4), is the first challenge to address the climate change problem. Zheng's study used various learning techniques, such as linear regression, support vector machines, and random forests to build an accurate model that would identify changes in the atmosphere's increasing temperature, dominated mainly by the increase in the temperature of CO_2 due to its higher concentration within greenhouse gases.

Different authors argue that the construction of a reliable model combined with the temperature dataset and machine learning prediction tools will help us to have a better understanding of the phenomenon, and thus be able to make a good forecast that allows us to face the risks of climate change. The thermal equilibrium model was studied by De Vos and Flater [28], who analyzed solar radiation as an energy converter used to examine the average temperature of a planet. It is carried out by the radiation from the planet's surface and the irradiance reaching Earth. This analysis takes into account the physical characteristics of the atmosphere, such as friendliness and the albedo effect [22,27,28]. Thus, the total flux Q appears as shown in Equation (2).

$$Q = 4\pi R^2 \sigma \left((1-\rho)\frac{f}{4}T_s^4 - (1-\gamma)T_p^4 \right) \tag{2}$$

It is the first thermodynamic model that allows for a dynamic study of the different layers of the atmosphere, with the lowest layer corresponding to the temperature on the planetary surface. This development can analyze various scenarios where greenhouse gases and albedo concentrations are modified. The feasibility of the model was tested in the study of geological eras, and several authors carried out the solution of the faint young Sun paradox [24,25]. The study of the solar converters under the regime of finite-time thermodynamics was analyzed in this work, changing the parameters to current time, considering the increase in CO_2 main greenhouse gas [36]; its relationship with albedo was developed too. In addition, a dissipation of energy in the system has realistic results at the current time.

According to the state of the art, there are several proposals related to analyzing global climate change based on prediction models developed with deep learning approaches, using specifically convolutional and recurrent neural networks. In [37], a method to efficiently predict weather forecasting was proposed by designing a model based on a convolutional neural network (CNN). Thus, Miloshevich et al. [38] proposed a methodology to create forecasting artifacts trained with data of 8000-year models, considering an infrastructure defined by a set of various CNNs, which was primarily focused on describing extreme heatwave datasets.

On the other hand, the CNN architecture has been widely employed to assess predictions between the hourly soil temperature and the subsurface depth. Thus, ref. [39] described a one-dimensional CNN prediction model to demonstrate that the air temperature and surface thermal radiation directly impact the soil temperature prediction model, affecting global warming.

Diverse studies have revealed that climate change rushes the increasing global temperature, causing a rise in the international sea level. Consequently, Hassan [40] implemented a set of different multivariable prediction models based on the principal deep learning techniques: recurrent neural networks (RNN), long short-term memory networks (LSTM), gated recurrent unit networks (GRU), and WaveNet as a particular case of CNN. The models used 29 years of data with multiple variables such as changes in the ocean heat content, level of carbon dioxide, mass variation in the Greenland and Antarctica regions, and global temperature anomalies.

According to Ghimire et al. [41], the use of a convolutional neural network with a multilayer perceptron (MLP) generates efficient forecasts of global solar radiation (GSR). The outcomes of their model achieved a relative error of less than 10%, generating a model with very high performance compared to climate models, especially in models developed with convective cells, such as Gordon and Zarmi-type models. Therefore, using CNN enriches the predictions of the climate models, inducing better forecasts that detect extreme weather events caused by climate change.

In consequence, the impact of climate change is reflected in the manifestation of extreme weather events such as droughts, floods, and heat waves. So, improving the methods for predicting global warming and its effects allows for adapting as a society to the planet's dynamic environment. An issue to analyze with climate change is its correlation with the hydroclimatic systems of the Earth. Larson et al. [42] proposed a deep convolutional residual regressive neural network to determine river basins' response to the water cycle's flows. The analysis revealed that this architecture and the catchment flow data exhibited satisfactory prediction performance for various locations at different time scales.

Natural disasters are related to climate change; some examples of these events include flash floods, droughts, and hurricanes. Thus, the Pacific Ocean weather phenomenon known as El Niño-Southern Oscillation (ENSO) is caused by cyclical changes in sea surface temperature (SST) and temperatures in the atmosphere near the tropics. The ENSO impact generates temperature variations, making them slightly warmer or colder up to extreme temperatures, inducing natural disasters. As claimed by Jonnalagadda and Hashemi [43], the use of the adaptive graph convolutional recurrent neural network (AGCRNN) can capture the temporal relationships of features with the Oceanic Niño Index (ONI), increasing the prediction time from three months to eighteen months, surpassing the current dynamic and statistical models.

In recent years, it has been observed that the automated detection of extreme weather events has increased. Therefore, it is required to improve the prediction performance to deal with these weather anomalies. Current research has shown that new convolutional neural network architectures enhance meteorological event detection. According to Lacombe et al. [44], the use of weighted loss functions counteracting the class imbalance in the data together with a correct architecture could show a significant improvement of the prediction up to 39.2% concerning events as natural cyclones. Due to the high impacts of extreme weather events, an energy transition that does not depend on the burning of fossil fuels, the main generator of greenhouse gases, is urgent. Photovoltaic power production is a good power generation option. However, this type of energy production is sensitive to weather, and can generate variations depending on weather conditions. To make realistic energy production forecasts, Ramakrishnan et al. [45] suggested a combined CNN and LSTM model, obtaining a better percentage of photovoltaic yield prediction, considering slow climate fluctuations and substantial climatic variations.

On the other hand, among the most significant consequences of climate change is related to the solar energy generation of power systems. Recently, the accuracy of intrahour solar forecasting has been a crucial topic to be analyzed in the field due to two critical aspects: (1) the accuracy of prediction models considering the dynamic coverage of clouds, and (2) the short forecast horizon for a minimal time window [46]. Thus, different proposals and methods to face these aspects have been proposed. Caldas and Alonso-Suárez [47] designed a hybrid model to predict solar irradiance, merging sky (cloud status) data provided by images and irradiance measures. The outcomes revealed that the model is efficient in preserving solar energy resources. In this sense, Pedro et al. [48] presented a study to compare machine learning algorithms such as k-nearest neighbors and gradient boosting in tasks to classify data based on intrahour forecasting and irradiance, taking information from sky images. Moreover, solar energy is the most favorable renewable source of electricity, employing a system based on a photovoltaic power supply. In [49], an artificial neural model was designed to predict solar irradiance values without using the detection of clouds.

3. Preliminary

3.1. Finite-Time Thermodynamics

The endoreversible Carnot machine is not in thermodynamic equilibrium with the reservoirs and the active substance. There is a separation between the internally reversible processes and the irreversibilities at the system boundaries, where internal processes with fast relaxation times can be considered reversible and the entropy change for the thermodynamic universe ΔS_u of the machine is positive, the entropy being of our null working substance $\Delta S_w = 0$. This definition is known as the endoreversibility hypothesis; when the model proposed by Curzon and Ahlborn [22] evolves in finite time, the model's power is nonzero, unlike that given by CET [50].

3.2. Curzon and Ahlborn Engine

The engine has thermal conductances that comply with Fourier's law for heat conduction ($\dot{Q} = -\lambda \nabla T$). In the present work, we will use the following notation to refer to the heat flows $Q = \dot{Q}$, such that:

$$Q_1 = \alpha(T_1 - T_{1w}) \tag{3}$$

$$Q_2 = \beta(T_{2w} - T_2) \tag{4}$$

A form of solution to the Curzon and Ahlborn [22] engine and the machine schematic was proposed in [27]. From the conservation of energy, we have the heat flow Q_1 from the upper reservoir, towards the reversible machine with power P to the output flow Q_2 [51]. By the entropic conservation of the system, $\Sigma S = 0$. Therefore, the production of entropy must be zero, whereas for the reversible internal machine, we assume that its entropy changes are zero (*endoreversibility hypothesis*) [23,28,51,52].

$$\sigma = \frac{Q_1}{T_1 w} - \frac{Q_2}{T_2 w} = 0 \tag{5}$$

From Equation (5) with the second law of thermodynamics, we have the following relationship for thermal conductors T_{1w} and T_{2w}.

$$T_{1w} = \frac{\alpha}{\alpha+\beta} T_1 + \frac{\beta}{\alpha+\beta} \frac{1}{1-\eta} T_2 \tag{6}$$

$$T_{2w} = \frac{\alpha}{\alpha+\beta}(1-\eta) T_1 + \frac{\beta}{\alpha+\beta} T_2 \tag{7}$$

Substituting T_{1w} in Equation (6) and T_{2w} in Equation (7) with our flow Q_1 and Q_2, we obtain Equations (8) and (9).

$$Q_1 = \gamma \frac{T_1 - T_2 - T_1\eta}{1-\eta} \tag{8}$$

$$Q_2 = T_2 \left(\frac{\beta(T_1(1-\eta) - T_2)}{\gamma(1-\eta)T_1 + \beta T_2} \right) \tag{9}$$

with the expression:

$$\gamma = \frac{\alpha\beta}{\alpha+\beta}$$

Thus, from the definition of efficiency, we can obtain an expression for the power given by:

$$P = \gamma \frac{\eta(T_1 - T_2 - T_1\eta)}{1-\eta} \tag{10}$$

Resulting in efficiency at maximum power for the Curzon–Ahlborn machine known in finite-time thermodynamics as η_{ca} that satisfies $0 < \eta_{ca} < \eta_c$.

$$\eta_{CA} = 1 - \sqrt{\frac{T_2}{T_1}} \tag{11}$$

In the endoreversible Curzon–Ahlborn model, the dissipation will be given by formulas that have been derived that show the efficiency of an engine under maximum power conditions [20,21].

$$\Phi_{rb} = Q_2 - \frac{T_2}{T_1} Q_1 \tag{12}$$

4. Materials and Methods

4.1. Gordon and Zarmi (GZ) Model

The atmospheric convection model proposed by GZ consists of a cell as an endoreversible Carnot cycle between two thermal reservoirs of extreme temperatures: the temperature T_1 is the working fluid (atmosphere) temperature at the lowest altitude in the system, related to the temperature of Earth's surface; the temperature in the highest part of the working fluid is the cold reservoir in the GZ model, and the temperature is related to the cosmic background radiation $T_2 = 3K$ (see Figure 2) [20]. The input energy is solar radiation, the active substance is the atmosphere, and the work performed by the fluid of the thermal machine is the mean power of the winds. The GZ convection cell consists of several components, including two isothermal branches where the atmosphere absorbs heat at lower altitudes. Additionally, two intermediate adiabatic branches are assumed to be instantaneous, and the remaining branch releases heat at higher altitudes into the universe [53]. The GZ maximizes the work per cycle W, subject to thermodynamic restrictions and the average solar radiation flux q_s [20,53].

$$\bar{q_s} = \frac{I_{sc}(1-\rho)}{4} \tag{13}$$

The GZ model works with a Sun–Earth–wind system as an endoreversible engine, in which the input heat is the solar radiation, the active substance is the atmosphere, and the labor produced by this cycle is the mean power of the winds. The cold store for this machine is outer space, with the temperature of the cosmic background radiation of 3K [20].

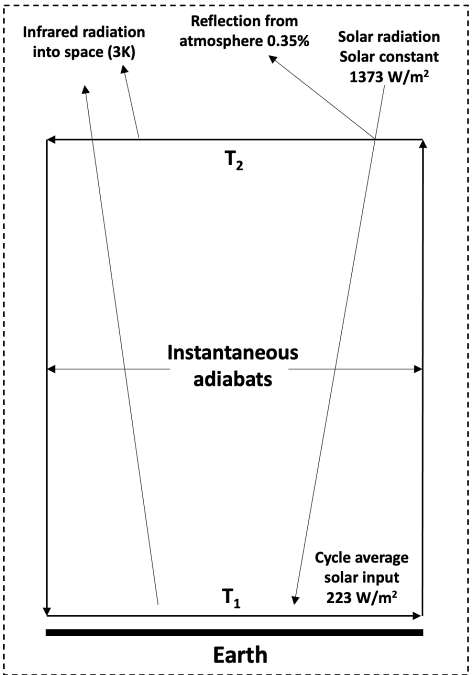

Figure 2. Simplified schema proposed by the GZ diagram of a cyclic heat engine driven by solar energy, the heat input is the solar radiation per area q_s, and the working fluid is the atmosphere. In contrast, the work output is the maximum wind energy. The model can obtain maximum and minimum temperatures of the atmosphere without considering any other effect on the Earth apart from the one already described in the convective cell [20].

Figure 2 shows a schematic view of the simplified system, including its isothermal and adiabatic branches. In addition, this diagram is a simplified version of a thermal engine driven by solar energy. The description of this figure is denoted as follows:

1. The atmosphere absorbs solar radiation at low altitudes through two isothermal branches. At the same time, heat is pushed out at high altitudes through another branch, in which the atmosphere rejects the excess heat.
2. There are two intermediate adiabats characterized by ascending and descending air currents, which occur instantaneously.

The temperatures associated with the four-cycle branches are as follows:

1. T_1 represents the temperature of the working fluid in the isothermal branch situated at the lowest altitude. Here, the working fluid absorbs solar radiation during every half cycle.
2. In the second half of the cycle, heat is released from the working fluid at temperature T_2 (at the highest altitude of the cell) through blackbody radiation, which is directed towards the cold reservoir at temperature T_{ex} (representing the 3K background radiation of the universe) [20,54].

The objective of this model is to maximize the work per cycle, equivalent to maximizing the average power output, according to certain thermodynamic restrictions. From the first law of thermodynamics for this model, we have the following:

$$\Delta U = -W + \int_{t=0}^{t=t_c} q_s(t) - \sigma[T^4(t) - T_e x^4(t)]dt = 0 \tag{14}$$

where ΔU is the change in internal energy of the active substance, σ is the Stefan–Boltzman constant ($5.67 \times 10^{-8} \frac{W}{m^2K^4}$), t_c is the cycle time, and T is the temperature of the active substance. The entropy change is subject to the endoreversibility restriction.

$$\Delta S = \int_{t=0}^{t=t_c} \left(\frac{q_s(t) - \sigma[T^4(t) - T_{ex}^4(t)]}{T(t)} \right) dt = 0 \tag{15}$$

The variables T, T_{ext} are functions associated with the time.

$$T(t) = \begin{cases} T_1 & 0 \leq t \leq t_c/2 \\ T_2 & t_c/2 \leq t \leq t_c \end{cases} \tag{16}$$

$$T_{ex}(t) = 3k \;\; 0 \leq t \leq t_c \tag{17}$$

The variable q_s is a function of time, I_{sc} is the average solar constant over the Earth's surface (1372.7 W/m^2), the average albedo $\rho = 0.35$, and the average values are as follows:

$$q_s(t) = \begin{cases} I_{sc}(1-\rho)/2 & 0 \leq t \leq t_c/2 \\ 0 & t_c/2 \leq t \leq t_c \end{cases} \tag{18}$$

$$\bar{T} = (T_1 + T_2)/2 \tag{19}$$

$$\bar{T^n} = (T_1^n + T_2^n)/2 \tag{20}$$

The mean power of the winds is obtained by:

$$P = \frac{W}{t_0} = \bar{q_s} + \sigma T_{ex}^4 - \sigma \bar{T}^4 \tag{21}$$

The model used by GZ considers the following approximation $\bar{q_s} >> \sigma T_{ex}^4$; we have the following Equation:

$$P = \bar{q_s} - \sigma \bar{T}^4 \tag{22}$$

From the endoreversibility condition, the variables T, T_{ex} and the mean values we obtained are:

$$\Delta S_{int} = \frac{\bar{q}_s}{T_1} - \frac{\sigma}{2}(T_1^3 + T_2^3) \tag{23}$$

To maximize P subject to the endoreversibility condition, the Lagrangian is defined in terms of the Lagrange multiplier λ and the thermodynamic constraint given by $L = P - \lambda \Delta S$, so that:

$$L = T^4(t) + \lambda[q_s(t)/T(t) - \sigma T^3(t)] \tag{24}$$

For finding the extreme of L, that is, solving $\frac{\partial L(t)}{\partial T(t)} = 0$, we have the following system of equations:

$$T_1^5(t) + 3\sigma\lambda T_1^4/4 - \lambda q_s(t)/4 = 0 \tag{25}$$

$$T_2^5(t) + 3\sigma\lambda T_2^4/4 = 0 \tag{26}$$

GZ found the following temperature values for the lowest and highest layers of the Earth's atmosphere $T_1 = 277K$, $T_2 = 192K$ and $P_{max} = 17.1\frac{W}{m^2}$. These values are not far from the literature $P_{max} = 7\frac{W}{m^2}$, $T_1 = 290K$ (on the surface) and $T_2 = 195K$ (between 75 and 90 km). Gordon and Zarmi [20] stated that their mean power of winds should be taken as an upper limit.

4.2. Nonendoreversibility Parameter in G-Z

In recent studies, the nonendoreversibility parameter R has been used to investigate the thermal machines of TTF. This parameter was introduced from the Clausius inequality, considering a clearance measure in the endoreversible regime [55].

$$\Delta S_{w1} + \Delta S_{w2} \leq 0 \tag{27}$$

ΔS_{w1} changes in the hot isotherm and ΔS_{w2} in the cold compression isotherm, in the endoreversible case. Thus, this inequality becomes equality in the following equation.

$$\Delta S_{w1} + R\Delta S_{w2} = 0, \tag{28}$$

where R is given by:

$$R = \frac{\Delta S_{w1}}{||\Delta S_{w2}||} \tag{29}$$

where $R = \frac{\Delta S_{w1}}{||\Delta S_{w2}||}$; the parameter of non-endoreversibility is in the interval $0 \leq R \leq 1$, where $R = 1$ is the endoreversible limit [51]. The previous GZ convection cell process is enriched using the parameter R. Thus, to maximize P subject to the endorreversibility condition plus the parameter R, the Lagrangean $L = P - \lambda \Delta S$ to occupy is given as follows:

$$L = \frac{\sigma}{2}(T_1^4 + T_2^4) + \lambda \left[\frac{\bar{q}_s}{T_1} - \frac{R\sigma(T_1^3 + T_2^3)}{2} \right] \tag{30}$$

Solving $\frac{\partial L(t)}{\partial T(t)} = 0$ to find the extrema of the Lagrangian; solving the system numerically, it is found that for a nonendoreversibility parameter $R = 0.953$ [55] for $\rho = 0.35$, $I_{sc} = 1372.7$ W/m^2. GZ found the following temperature values for the lowest and highest layers of the Earth's atmosphere $T_1 = 280.562K$, $T_2 = 194.293K$.

5. The Proposed Model

5.1. Greenhouse Factor

The planet's surface temperature computation is modified by adding the greenhouse parameter γ. Therefore, it is necessary to add the greenhouse effect to the equations proposed by the thermodynamics of finite times, to obtain the temperatures of the lower and upper layers of our active substance (in this case, the air). Thus, the equations for entropy and internal energy are also changed.

$$\Delta U = -w + \int_{t=0}^{t=t_c} q_s(t) - \sigma(1-\gamma)[T^4(t) - T_e x^4(t)]dt = 0 \tag{31}$$

Equation (15) is expressed in terms of the nonendoreversibility parameter and the greenhouse factor, giving as a result the following expression:

$$\Delta S = \int_{t=0}^{t=t_c} \left(\frac{q_s(t) - R(1-\gamma)\sigma[T^4(t) - T_{ex}^4(t)]}{T(t)} \right) dt = 0 \tag{32}$$

From the G-Z section, the average power of the winds $P = \frac{w_c}{t}$, in which $\bar{q}_s >> \sigma T_{ex}^4$, the power expression output for the case of the greenhouse effect is of the form:

$$P = \bar{q}_s - \frac{\sigma}{2}(1-\gamma)[T_1^4 + T_2^4] \tag{33}$$

Equations (31) and (32) show us a greenhouse factor acting on the two layers of the atmosphere with temperatures T_1 and T_2. To maximize P subject to the endoreversibility condition, we defined the Lagrangian in terms of the Lagrange multiplier λ and the thermodynamic constraint given by $L = P - \lambda \Delta S$, so that:

$$L = \bar{q}_s - \frac{\sigma}{2}(1-\gamma)[T_1^4 + T_2^4] - \lambda \left\{ \frac{\bar{q}_s}{T_1} - \frac{\sigma}{2}(1-\gamma)[T_1^3 + T_2^3] \right\} \tag{34}$$

where λ is a Lagrange multiplier. By solving the Euler–Lagrange equations $\frac{\partial L(t)}{\partial T(t)} = 0$, a system of equations is obtained, which allows us to calculate the extremes of the power.

For $\frac{\partial L(t)}{\partial T_1(t)} = 0$:

$$T_1^5 - \frac{3}{4} R \lambda T_1^4 - \frac{\bar{q}_s}{2\sigma(1-\gamma)} = 0 \tag{35}$$

For the case $\frac{\partial L(t)}{\partial T_2(t)} = 0$:

$$T_2 = \frac{3R}{4}\lambda \tag{36}$$

Finally, for $\frac{\partial L(t)}{\partial \lambda} = 0$ we have:

$$\frac{\bar{q}_s}{T_1} - \frac{\sigma}{2}(1-\gamma)[T_1^3 + T_2^3] = 0 \tag{37}$$

Eliminating λ and giving the value of $q_s \approx 229\ \mathrm{W/m^2}$ [50], we have two equations whose numerical solution provides the highest and lowest layer surface temperatures. The low of the Earth's atmosphere is under a regime of maximum power in terms of the nonendoreversibility parameter R, the albedo ρ, the greenhouse effect γ, and the current solar constant $I_s c$.

$$T_1^5 - T_2 T_1^4 - \frac{2q_s}{3R\sigma(1-\gamma)} T_2 = 0 \tag{38}$$

$$T_1^4 + T_2^3 T_1 - \frac{2\bar{q}_s}{R\sigma(1-\gamma)} = 0 \tag{39}$$

5.2. Greenhouse Factor in the Lowest Layer of the Atmosphere Average Surface Temperature

The power for the G-Z model is given by $P = \frac{w_c}{t}$, where for $T_{ex} = 3K\,\bar{q}_s >> \sigma T_{ex}^4$, the output power expression with the greenhouse effect in the lower part is the following:

$$P = \bar{q}_s - \frac{\sigma R}{2}[(1-\gamma)T_1^4 + T_2^4] \tag{40}$$

It is necessary to maximize P subject to the endoreversibility condition and the greenhouse effect at the bottom. Then, the Lagrangian is defined in terms of the Lagrange multiplier λ and the constraint on thermodynamics showing the following Lagrangian expression:

$$L = \bar{q}_s - \frac{\sigma}{2}[(1-\gamma)T_1^4 + T_2^4] - \lambda\left\{\frac{\bar{q}_s}{T_1} - \frac{\sigma}{2}[(1-\gamma)T_1^3 + T_2^3]\right\} \tag{41}$$

Solving the Euler–Lagrange equations $\frac{\partial L(t)}{\partial T(t)} = 0$, we obtain the following equations:

For $\frac{\partial L(t)}{\partial T_1(t)} = 0$:

$$T_1^5 - \frac{3}{4}R\lambda T_1^4 - \frac{\bar{q}_s}{2\sigma(1-\gamma)} = 0 \tag{42}$$

For $\frac{\partial L(t)}{\partial T_2(t)} = 0$:

$$T_2 = \frac{3R}{4}\lambda \tag{43}$$

For $\frac{\partial L(t)}{\partial \lambda} = 0$, we have:

$$\frac{\bar{q}_s}{T_1} - \frac{\sigma}{2}[(1-\gamma)T_1^3 + T_2^3] = 0 \tag{44}$$

Removing the λ parameters from Equations (42)–(44), we obtain:

$$T_1^5 - T_2 T_1^4 - \frac{2\bar{q}_s}{3R\sigma(1-\gamma)}T_2 = 0 \tag{45}$$

$$T_1^4 + \frac{1}{(1-\gamma)}T_2^3 T_1 - \frac{\bar{2}q_s}{R\sigma(1-\gamma)} = 0 \tag{46}$$

The FTT models are developed as engines that use the conversion of solar energy into wind energy; the hypothesis is that atmospheric work as a "heat engine" provides reasonable values for the average power of winds and extreme temperatures in specific layers of the atmosphere. To compute the efficiency of the energy converter, it is necessary to take the average power output associated with the yearly average solar radiation flux q_s expressed per unit area of the Earth's surface (see Equation (47)). Therefore, solar energy efficiency or performance is defined as $w = P/q_s$.

$$w = \frac{(1-\gamma)(R-1) + R^4(1-\eta)^3[1-R(1-\eta)]}{R[(1-\gamma) + R^3(1-\eta)^3]} \tag{47}$$

Thus, for the endoreversible case $R = 1$:

$$w = \frac{\eta(1-\eta)^3}{(1-\gamma) + (1-\eta)^3} \tag{48}$$

Equation (48) shows us that even for an endoreversible case, the efficiency of solar energy depends on the greenhouse effect. For a regime at maximum power for $\gamma = 0$, 7.67% of the solar energy q_s can be converted into energy, regardless of the planet and the solar system.

Nevertheless, it does not represent a realistic model of the atmosphere of the planets. The model can be extended by considering other thermodynamic regimes, such as the ecological and efficient power regimes. Other conditions, such as physical and geometric issues about the planet, improve our thermal engine, which implies more accurate predictions. According to the model developed by De Vos and Flatter [27], they obtained a value $\omega = 9.64\%$ whereas a Hadley-type considers a convection cell and divides the planet into two hemispheres, thus generating different heat exchanges where radiation is received or emitted from their surface areas.

The models proposed by De Vos as well as Gordon and Zarmi [20,27] can compute the temperatures of the atmosphere of some past or future periods of the Earth, as was carried out in the study by Angulo and Barranco-Jiménez [24], where the temperatures of early age were calculated with enough accuracy. In the present work, we worked similarly, but for a future time of the atmosphere (prediction event), we considered the atmosphere's physical characteristics, such as the albedo greenhouse effect. The model created by De Vos shows an excellent relationship between the theoretical and experimental data. Our proposed work approximated the albedo dependent on the greenhouse effect with $a = 0.072$, $b = 0.4955$, and $c = 0.1527$.

$$\rho = a\gamma^2 + b\gamma + c \tag{49}$$

The GZ-type models with the greenhouse factor and the albedo condition above, and the atmosphere represented by Equations (45) and (46), allow us to obtain temperatures of the highest and lowest layers of the atmosphere. It is necessary to determine the atmospheric characteristics of the GZ-type models. According to the solution of the faint young Sun paradox presented in [24], the finite-time thermodynamics models efficiently resolve the paradox, calculating the planet's average surface temperature from different geological stages. Using scenarios where the luminosity of the Sun is taken into account through the Gough Equation (1), it is necessary to modify this equation to actual luminosity, as represented in Equation (50).

$$I(t) = \left[1 + 0.4\left(1 - \frac{t + t_0}{t_0}\right)\right]^{-1} I_{sc} \tag{50}$$

Using the albedo ρ (Equation (49)), the average solar radiation flux, and greenhouse coefficient γ, we modified the scheme proposed by Angulo and Barranco to determine the effects of climate change due to the increase in greenhouse gas, taking the relationship proposed in our work. That relationship between the albedo and greenhouse effect is represented in Equation (49), including the present-day values for average luminosity, its variation per year (Equation 50), and the changes directly proportional to the flux q_s expressed in Equation (13). Nevertheless, it is necessary to consider the dissipation in the maximum power regime to obtain realistic results. This modification allows results to be obtained to predict the effects of climate change in future years. Thus, the average temperature of the surface (T_s) at present will be based on the existing relationship in the dissipation (Equation (12)) of the system in maximum-power conditions in the GZ-type model with Equations (45) and (46).

$$T_s = T_1 + T_2\left(\frac{\beta(T_1(1-\eta_{CA}) - T_2)}{\gamma(1-\eta_{CA})T_1 + \beta T_2}\right) - \frac{T_2\gamma(T_1 - T_2 - T_1\eta_{CA})}{T_1(1-\eta_{CA})} \tag{51}$$

Simplifying:

$$T_s = T_1 + T2\left(\frac{T1(1-\eta_{CA}) - T2}{(1-\eta_{CA})T1 + T2}\right) - \frac{T_2}{T_1}\left(\frac{(T1 - T2 - T1\eta_{CA})}{(1-\eta_{CA})}\right) \tag{52}$$

6. Experimental Results

It is necessary to determine possible and future scenarios for the growth of greenhouse gases. Most of the concentration of gases in the atmosphere has presented a significant increase since the 1970s due to industrial activities. According to the Mauna Loa laboratory in Hawaii [53,56], the data show a massive rise in CO_2 by the empirical formula concentration for the interval $1975 \leq t \leq 2100$ [53]. So, the expression obtained by Wubbles concerning the trace gas trends and their potential role in climate change is valid for this methodology [53].

$$[CO_2] = 330^{e^{0.0056(t-1975)}} \tag{53}$$

According to Equation (49), the albedo and the greenhouse effect are related. For the Earth, the value of the greenhouse effect can be defined as $\gamma = (E_s - F)/E_s$, where E_s is the surface emission and F is the outgoing radiation [24]. Moreover, it is noticed that the increase in greenhouse gases rises over time, according to Wubbles and different experimental measurements. With all these characteristics, the natural average temperature (T_s) and its possible evolution in the coming years can be determined with reasonable accuracy. To test the GZ model, a dissipation ϕ_{rb}, developed in this work, is considered, solving numerically with $R = 1$ and different values of γ are related to the year. It is a data compilation by Berkeley Earth. The study shows the temperature of the Earth's surface, and the experimentally measured temperatures T_{obs} were compared against our theoretically calculated temperatures T_s to use a forecasting technique later to determine the future of temperatures.

On the other hand, the comparison was made using machine learning techniques such as linear regression, Ridge regression, and artificial neural networks. Concerning the implementation, we used the Scikit-learn framework for regression methods and the TensorFlow package with Keras for designing the artificial neural network. The parameters for the artificial intelligence-based approach were described according to the formalism of Scikit-learn and TensorFlow Keras. Thus, the setup parameters and configuration were established as follows:

- **Linear regression**: `train_size = X_train, X_test, y_train, y_test = train_test_split(X, y, train_size = 0.8)`
- **Ridge regression**: `train_size = X_train, X_test, y_train, y_test = train_test_split(X, y, train_size = 0.8)`
- **Neural network optimizer** was implemented by applying Adam's algorithm. The regression loss was defined by `MeanSquaredError`. Moreover, four layers were established with the activation functions: `linear, linear, relu, linear`.

Data Preprocessing

To analyze the complexity of climate change, the terrestrial and oceanic temperatures of the planet were measured. The used data are a compilation of a dataset provided by Berkeley Laboratory. Other widely used datasets are MLOST NOAA Land-Ocean Surface Temperature and GISTEM from NASA [57–59]. The data compilation by Berkeley records land average temperatures in the format yyyy/mm/dd. So, a split was made by year, month, and day, taking the temperature of each month, and the mean temperature per year was computed. It was observed that there is a correlation with a value of 0.89 between the variables of the year and the land average temperature from the year 1975 to 2015 [57–59]. Figure 3 shows the climatology of the average annual terrestrial temperature between 1951 and 1980 from the Berkeley Earth Data with a global mean of 9.17 Celsius. In our work, the mean experimental temperature of each year was compared with the obtained data from our theoretical model.

The results of the data and the surface temperatures T_s obtained from the model expressed in Equation (52) that was developed in this work are shown in Table 1. All the results regarding data are presented in degrees Celsius.

Table 1. Average temperatures observed and computed by the GZ-type model.

Year	T_{obs}	T_s
1975	8.74	8.41
1976	8.34	8.44
1977	8.85	8.48
1978	8.69	8.51
1979	8.73	8.55
1980	8.98	8.58
1981	9.16	8.62
1982	8.63	8.65
1983	9.02	8.69
1984	8.65	8.73
1985	8.65	8.77
1986	8.83	8.80
1987	8.99	8.84
1988	9.20	8.88
1989	8.922	8.92
1990	9.23	8.96
1991	9.17	9.00
1992	8.83	9.04
1993	8.86	9.08
1994	9.03	9.12
1995	9.34	9.16
1996	9.03	9.21
1997	9.20	9.24
1998	9.52	9.29
1999	9.28	9.33
2000	9.20	9.37
2001	9.41	9.38
2002	9.57	9.46
2003	9.52	9.50
2004	9.32	9.48
2005	9.70	9.59
2006	9.53	9.64
2007	9.73	9.73
2008	9.43	9.74
2009	9.50	9.78
2010	9.703	9.82
2011	9.51	9.87
2012	9.507	9.92
2013	9.606	9.97
2014	9.570	10.02
2015	9.831	10.07

The temperature increase due to greenhouse gas growth has been analyzed since 1975. It was fixed this year because of the significant increase in the concentration of CO_2, as shown by the experimental development of Wubbles in Equation (53), when seeing the correlations of the observational variables of the temperature of the Berkeley database. We can notice a high correlation between the year and the land's average temperature, and the correlation is equal to 0.89. Therefore, a linear regression model is sufficient in this case to make a future prediction of the temperature. In the following plot (Figure 4, average temperatures observed and calculated by the GZ-type model), we can observe a relationship between the average temperature per year measured against the temperature of the modified GZ model.

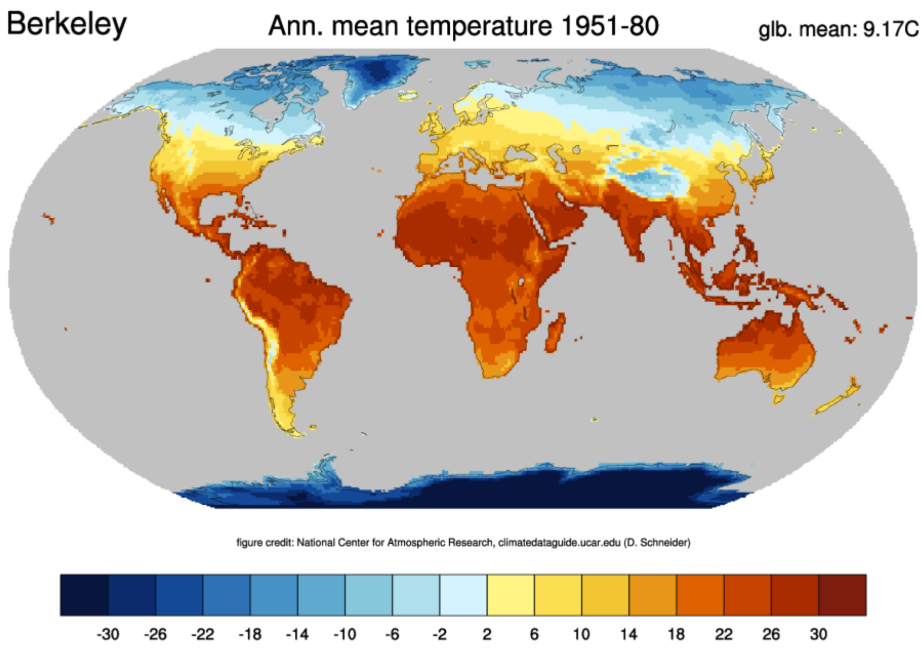

Figure 3. Climatology of annual mean land temperature. NCAR, Climate Data Guide [59].

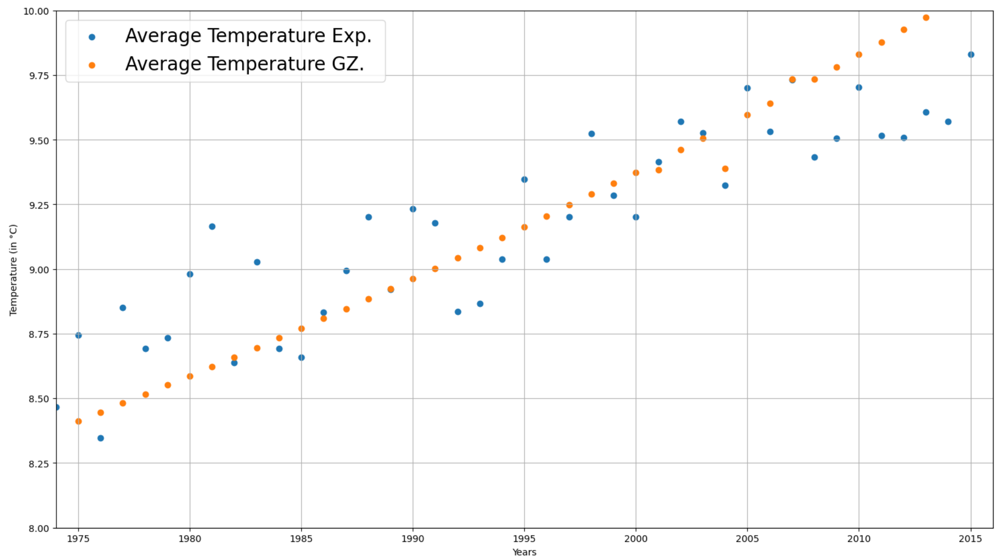

Figure 4. Average temperatures observed and computed by the GZ-type model compared with the average measured yearly temperature.

Thus, (Figure 5, average temperatures observed since 1975 with linear regression) shows how a linear regression adjusts perfectly to predict the evolution of the temperature from the year 1975. It is possible to infer how the temperature change will be towards the year 2100 thanks to this type of modeling.

On the other hand, Table 2 presents the future prediction of the temperatures using linear regression (LR), ridge regression (RR), and an artificial neural network (ANN). Thus, the ANN has five layers: an input layer with a linear activation function; three layers with a rectified linear activation function, or *Relu* or *ReLU* for short; and an output layer with a linear activation function. All techniques were applied to the observed temperatures (T_{obs}) and the models' temperatures used in the present work. In the same way, the third column shows the temperatures computed (T_s) from our model of Gordon and Zarmi (GZM) without applying a linear regression, where the physical characteristics of the atmosphere are taken into account and what theoretical temperature would be reached. In addition, Table 2 depicts the entire prediction made up to 2100, starting in 2016.

Table 2. Average temperatures observed and computed by the GZ type model.

Year	T_{obs} with LR	T_s with LR	T_{obs} with RR	T_{obs} with NN	T_s with GZM
2016	9.839	10.049	9.845	10.089	10.121
2017	9.842	10.094	9.860	10.094	10.176
2018	9.845	10.135	9.869	10.099	10.228
2019	9.860	10.178	9.884	10.105	10.281
2020	9.885	10.219	9.907	10.110	10.334
2021	9.913	10.251	9.937	10.115	10.387
2022	9.941	10.292	9.967	10.120	10.440
2023	9.969	10.333	9.996	10.125	10.495
2024	9.997	10.374	10.026	10.130	10.550
2025	10.025	10.426	10.056	10.135	10.606
2026	10.053	10.456	10.086	10.140	10.663
2027	10.081	10.497	10.116	10.144	10.720
2028	10.109	10.538	10.146	10.149	10.777
2029	10.137	10.579	10.175	10.154	10.836
2030	10.165	10.620	10.205	10.159	10.895
2031	10.193	10.661	10.235	10.164	10.954
2032	10.221	10.702	10.265	10.169	11.014
2033	10.249	10.743	10.295	10.174	11.018
2034	10.277	10.784	10.325	10.179	11.138
2035	10.305	10.825	10.354	10.184	11.200
2036	10.333	10.866	10.384	10.189	11.263
2037	10.361	10.907	10.414	10.194	11.327
2038	10.389	10.948	10.444	10.199	11.392
2039	10.417	10.989	10.474	10.204	11.456
2040	10.445	11.030	10.504	10.209	11.524
2041	10.473	11.071	10.533	10.213	11.591
2042	10.501	11.112	10.563	10.218	11.659
2043	10.529	11.153	10.593	10.223	11.728
2044	10.557	11.194	10.623	10.233	11.798
2045	10.585	11.235	10.653	10.238	11.868
2046	10.613	11.276	10.683	10.243	11.939
2047	10.641	11.317	10.713	10.246	12.012
2048	10.669	11.358	10.742	10.248	12.085
2049	10.697	11.399	10.772	10.253	12.159
2050	10.725	11.440	10.802	10.258	12.234
2051	10.753	11.481	10.832	10.263	12.311
2052	10.781	11.522	10.862	10.268	12.388
2053	10.809	11.563	10.892	10.272	12.465
2054	10.837	11.604	10.921	10.277	12.545
2055	10.865	11.645	10.951	10.282	12.625
2056	10.893	11.686	10.981	10.287	12.707
2057	10.921	11.727	11.011	10.292	12.789
2058	10.949	11.768	11.041	10.297	12.872
2059	10.977	11.809	11.071	10.302	12.957
2060	11.005	11.850	11.100	10.307	13.043
2061	11.033	11.891	11.130	10.312	13.129
2062	11.061	11.932	11.160	10.317	13.218
2063	11.089	11.973	11.190	10.322	13.308
2064	11.117	12.014	11.220	10.327	13.398
2065	11.145	12.055	11.250	10.332	13.490
2066	11.173	12.096	11.279	10.336	13.584
2067	11.201	12.137	11.309	10.341	13.659
2068	11.229	12.178	11.339	10.346	13.775
2069	11.257	12.219	11.369	10.351	13.872

Table 2. *Cont.*

Year	T_{obs} with LR	T_s with LR	T_{obs} with RR	T_{obs} with NN	T_s with GZM
2070	11.285	12.260	11.399	10.356	13.972
2071	11.313	12.301	11.429	10.361	14.072
2072	11.341	12.342	11.458	10.366	14.174
2073	11.369	12.383	11.488	10.371	14.277
2074	11.397	12.424	11.518	10.376	14.383
2075	11.425	12.465	11.548	10.381	14.490
2076	11.453	12.506	11.578	10.386	14.599
2077	11.481	12.547	11.608	10.390	14.709
2078	11.509	12.588	11.637	10.396	14.820
2079	11.537	12.629	11.667	10.401	14.935
2080	11.565	12.670	11.697	10.405	15.050
2081	11.593	12.711	11.727	10.410	15.168
2082	11.621	12.752	11.757	10.415	15.287
2083	11.649	12.793	11.787	10.420	15.408
2084	11.677	12.834	11.816	10.425	15.533
2085	11.705	12.875	11.846	10.430	15.658
2086	11.733	12.916	11.876	10.435	15.786
2087	11.761	12.957	11.906	10.440	15.916
2088	11.789	12.998	11.936	10.445	16.048
2089	11.817	13.039	11.966	10.450	16.183
2090	11.845	13.080	11.995	10.455	16.320
2091	11.873	13.121	12.025	10.460	16.460
2092	11.901	13.162	12.055	10.465	16.601
2093	11.929	13.203	12.085	10.469	16.746
2094	11.957	13.244	12.115	10.474	16.894
2095	11.985	13.285	12.145	10.479	17.043
2096	12.013	13.326	12.174	10.484	17.196
2097	12.041	13.367	12.204	10.489	17.352
2098	12.069	13.408	12.234	10.494	17.511
2099	12.097	13.449	12.264	10.499	17.673
2100	12.125	13.490	12.294	10.504	17.838

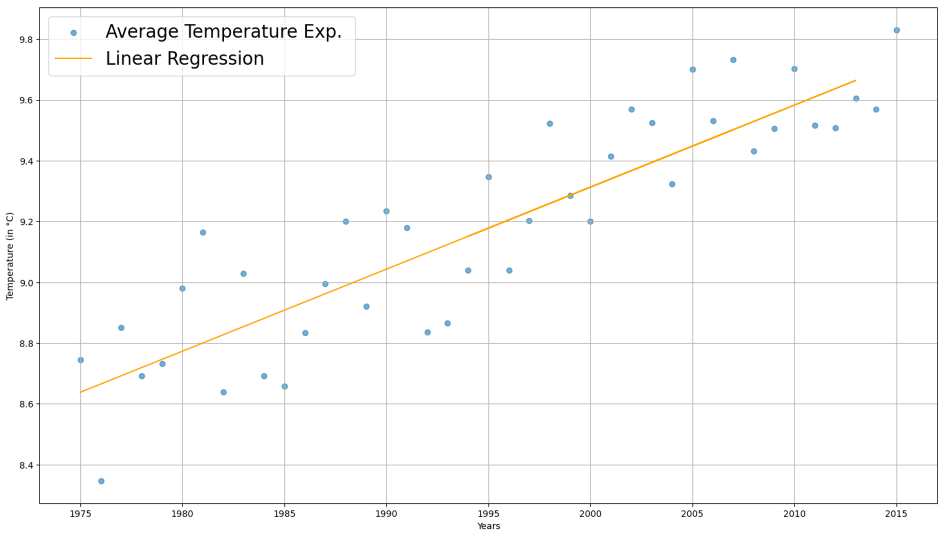

Figure 5. Average temperatures observed since 1975 with linear regression adjusted to predict the rise of mean temperature.

Moreover, Figure 6 shows the evolution of the surface temperature (T_s), according to the predictions made by the model proposed in our work with the initials GZM and the temperature prediction from the experimental data (T_{obs}). Thus, T_S and T_{obs} were forecasted using machine learning techniques.

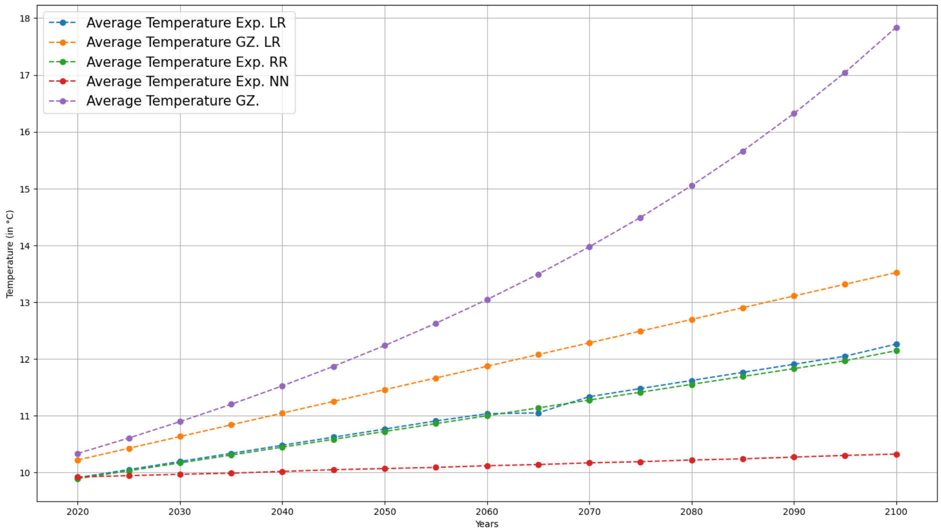

Figure 6. Comparison of the evolution of temperature from the year 2020 to 2100 through theoretical and experimental models.

From a correlation analysis between the temperature variables under different machine learning techniques, such as linear regression (LR), ridge regression (RR), artificial neural network (ANN), and the proposed endoreversible model (GZM), it can be observed that the GZM model is more suitable with a linear relationship (see Figure 7).

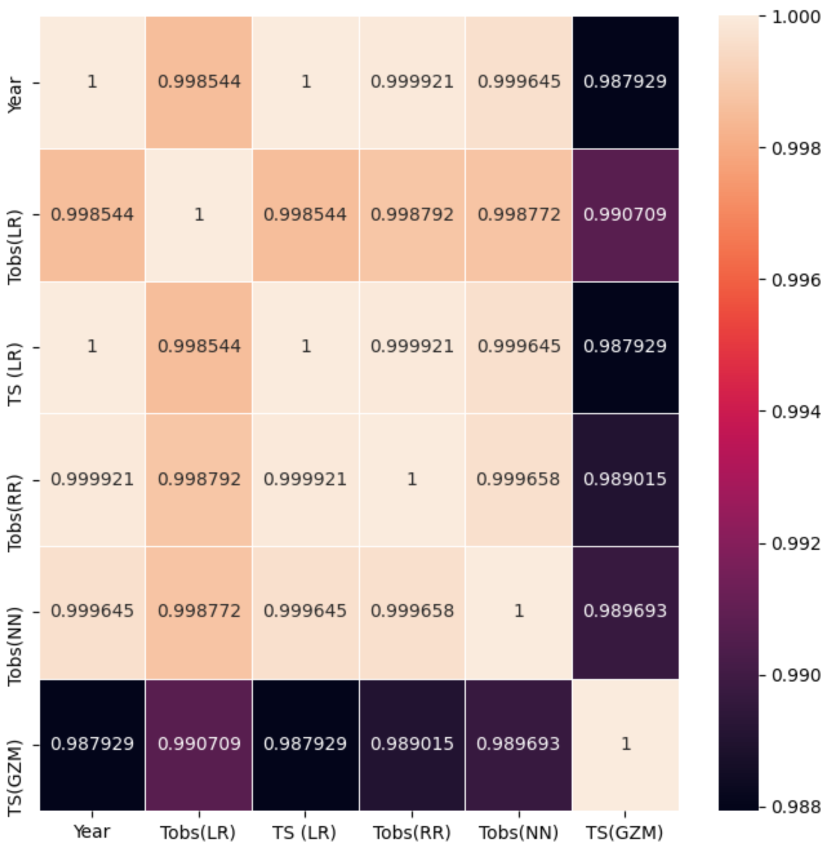

Figure 7. Comparison of the correlation between year variables and observed temperatures with the theoretical model.

7. Discussion

According to several authors, the changes in the concentration of gases in the atmosphere, mainly greenhouse gases, in addition to their directed relationship with the albedo effect, are related to climate change [24,29,60,61].

Climate model development and the implications in a model's prediction reliability can be difficult, because the climate is a complex system with many variables and factors. The models are fully coupled when studying a complete interaction among the global radiation budget, different layers of the atmosphere, physical and chemical atmospheric processes, and their implications in the biosphere. The models are considered partially coupled and developed in a system of Sun–atmosphere–ocean. Differential equations represent the governing equations that describe atmospheric and ocean circulation, geophysical fluid dynamics, continuity equations, the input of solar radiation, and physical thermodynamic processes [29,61–65]. Therefore, global climate models can have many degrees of freedom.

Nevertheless, these models are very complex and expensive to solve through analytical and computational methods. Thus, the nonlinearity leads to multiple solutions that must be carefully analyzed to find physically acceptable results and predictions. A method used to work with these chaotic systems is the use of approximations or attractors, the use and development of simplified climate models, or the linearization of global climate models [29,65–67].

In this work, we used a climate model based on the Gordon–Zarmi approach, where the system is represented like a heat engine that describes an Earth–atmosphere–Sun system, providing reasonable values of extreme temperatures in the layers of the atmosphere. The model solved the paradox of the young and weak Sun, proposing a series of scenarios with the different greenhouse effect and albedo values, taking into account the luminosity of the Sun and the evolution of these values over time. These variables are responsible for generating global warming, and the obtained prediction is correlated with the estimated warming values from experimental data.

According to Houghton et al. [29], it is essential to note that since the climate is a chaotic system, its predictions become very complicated, so using climate models and predictions made from experimental data through numerical techniques or machine learning help to provide robustness to future predictions.

In this analysis of climate change, an endoreversible modeling of the Gordon and Zarmi type was carried out. Unlike other finite-time thermodynamic studies for studying the atmosphere, adjustments were made to give the model realistic results if applied. As for the climatic analysis of geological eras, as observed in other works, it is noticed that the results do not correspond to what is reported by observations of the current temperature. According to Levario et al. [21], for a correct thermodynamic optimization of power plants, it is necessary to consider the system's variations. Therefore, the modeling was performed considering those variations, the change in luminosity per year, the increase in greenhouse gas, and its relationship with the terrestrial albedo, thus adapting it to our model of winds at maximum power. In this way, the family from Equation (45) to Equation (53) complements the system to calculate climate change due to atmospheric conditions and the increase in greenhouse gases by anthropogenic conditions.

From Table 1, an increase in the average temperature of the Earth's surface can be seen from 1975 to 2015, both in the observational (experimental) model and the theoretical model developed in our work. The rise in temperature in both cases is related to the increase in greenhouse gases in the atmosphere.

In Figure 2, we can appreciate the differences between the points obtained experimentally (observation and measures in the laboratory) and the modeling proposed in our work. Suppose we observe Figure 3 and correlation analysis; in that case, the experimental points in blue show a high linear tendency, so linear or ridge regression is an excellent technique for correctly predicting temperature increases.

On the other hand, the points of our previously mentioned modeling of the GZM would seem to show the same linear trend, so in Table 2, two comparisons were made, taking into account a linear regression with T_s **LR** and an analysis obtained directly from our modeling with T_s **GZM**. As a result, we obtained a difference between the analysis with LR and GZM. This is explained considering that the temperature observations only recorded points in our vector. In contrast, the modeling records these points, and the physical information of the atmosphere is saved, as well as the thermodynamic variables of the system, which gives us results of the mean temperature increase with more value than those obtained by an analysis of experimental points.

Moreover, Figure 4 shows a plot of the predictions made from the experimental data T_{obs} and the modeling of the GZM system. It is important to note that in future scenarios with forecasting by GZM, the average temperature is higher than that obtained by the data of the evolution of the observed temperatures T_{obs} from various machine learning techniques. Nevertheless, the rate of temperature increase is in the range per decade, according to [29]. The plot shows that the temperature evolution in the case of the construction of an ANN, LR, and RR grows in a widespread gradual way compared with our proposed model. The GZM model saves the atmosphere's physical characteristics, such as entropic relationships, radiation conditions, and irradiance. It helps to present more realistic behavior in the data, unlike the other forecasting, which only shows us a regression of the linear type without considering the evolution of the physical parameters caused by the alterations in the Earth's atmosphere.

The most significant challenge for developing a sun model is establishing a critical finite-time thermodynamics condition. Developing objective functions that characterize the "optimal" modes of operation is not a trivial task. However, there are no established criteria to set the objective functions, so the objective of the modeling itself is the one that affects the construction of the "heat engine", in addition to affecting its behavior in the energy converter and its performance [68].

Solar energy converters under the branch of FTT have been developed to create models with better coupled experimental and theoretical results. These energy converters are focused on entropy minimization and output power maximization, among others. According to De Vos [28], the Curzon and Ahlborn engine is valid when the heat transfer is linear or Newtonian, so another challenge related to these modeling types is to work the heat transfer linearly.

8. Conclusions and Future Work

In this article, we proposed a new finite-time thermodynamics approach to predict changes in surface temperature in the lowest layer of the atmosphere that corresponds to the average temperature. The proposed approach considers the evolution in albedo and greenhouse gases, the change in luminosity per year, and the system's dissipation in the regime of maximum-power conditions. Our model achieves predictions in the range of future projections, obtaining better results than the machine learning techniques used in the experiments. Another area for improvement is that it performs a simple climate model, avoiding the complexity of modeling the climate as a chaotic system. The current modeling is a modification of previous models of the GZ type that, in addition to obtaining realistic values of the extreme temperatures of the system, also allows us to carry out the evolution of temperatures according to the modifications of the physical processes of the planet in a rate of change of time.

Thus, an increase in temperature is linked to physical conditions such as irradiance and radiation. Moreover, a comparison with different machine learning techniques showed a rise in temperature in all these methods. It is crucial to notice that machine learning algorithms do not preserve atmospheric information in the period studied. Therefore, the forecasting could present a *bias* in the prediction because these are trained only with experimental data without considering the variables that generate climate change. The comparison gives robustness to the model when comparing the experimental data with the theoretical ones. As mentioned previously, due to the high degrees of freedom of the climate model, interdisciplinary works are necessary to face new challenges in climate warming. All the techniques and our modeling demonstrated an increase in temperature. We can conclude the success of our model by comparing it with our experimental data. In addition, according to Houghton [29], the projections of global average temperature changes are in the range of 0.15 °C–0.6 °C per decade, which is in the threshold of the obtained values.

In the present work, the endoreversible engines of FTT deal with the problem of the radiative thermal balance between planets, generating a Sun–Earth–wind system through an atmospheric heat engine that allows for the optimization of the extreme values of the model to find the maximum output power and entropy minimization, among others. Thus, these values allow us to work under different thermal regimes of the FTT, namely the maximum power regime (MPR), maximum ecological regime (MER), and maximum efficiency power (MEPR). This model was created under the MER regime. According to several authors, to fully model, it is necessary to generalize various cases and verify experimental data due to climate variability as a subject of study. Therefore, an extension of our research work would be to analyze the other thermodynamic regimes. We have to propose several cases of increases in greenhouse gases and the albedo effect, compare them with the experimental data, and complement them with deep learning techniques. All theoretical predictions will always be compared against experimental data to face climate change in the best way.

On the other hand, it is necessary to conduct studies concerning the atmosphere and consider a wind engine the most common control in obtaining the maximum power as it works, collecting data from these experiments and generating machine learning models to characterize the phenomenon. In this paper, studying other regimes will allow us to analyze the whole spectrum of our modeling (wind engine) and thus observe all cases of global warming.

Author Contributions: Conceptualization, S.V.-R. and M.T.-R.; methodology, R.Q.; software, C.G.S.-M. and K.T.C.; validation, S.V.-R. and M.T.-R.; formal analysis, R.Q. and S.V.-R.; investigation, M.T.-R.; resources, K.T.C.; data curation, C.G.S.-M.; writing—original draft preparation, S.V.-R.; writing—review and editing, M.T.-R.; visualization, K.T.C.; supervision, M.T.-R.; project administration, C.G.S.-M.; funding acquisition, K.T.C. All authors have read and agreed to the published version of the manuscript.

Funding: This work was partially sponsored by the Instituto Politécnico Nacional and the Consejo Nacional de Ciencia y Tecnología under grants 20230655, 20231372, and SECTEI-2023, respectively.

Institutional Review Board Statement: Not applicable.

Informed Consent Statement: Not applicable.

Data Availability Statement: Not applicable.

Acknowledgments: We are thankful to the reviewers for their time and their invaluable and constructive feedback that helped improve the quality of the paper.

Conflicts of Interest: The authors declare no conflict of interest.

References

1. Kirilenko, A.P.; Sedjo, R.A. Climate change impacts on forestry. *Proc. Natl. Acad. Sci. USA* **2007**, *104*, 19697–19702. [CrossRef] [PubMed]
2. Carleton, T.A.; Hsiang, S.M. Social and economic impacts of climate. *Science* **2016**, *353*, aad9837. [CrossRef] [PubMed]
3. Wheeler, T.; Von Braun, J. Climate change impacts on global food security. *Science* **2013**, *341*, 508–513. [CrossRef] [PubMed]
4. Louis, M.E.S.; Hess, J.J. Climate change: Impacts on and implications for global health. *Am. J. Prev. Med.* **2008**, *35*, 527–538. [CrossRef] [PubMed]
5. Nourani, V.; Tapeh, A.H.G.; Khodkar, K.; Huang, J.J. Assessing long-term climate change impact on spatiotemporal changes of groundwater level using autoregressive-based and ensemble machine learning models. *J. Environ. Manag.* **2023**, *336*, 117653. [CrossRef]
6. Yeganeh-Bakhtiary, A.; EyvazOghli, H.; Shabakhty, N.; Kamranzad, B.; Abolfathi, S. Machine learning as a downscaling approach for prediction of wind characteristics under future climate change scenarios. *Complexity* **2022**, *2022*, 8451812.

7. Rajaee, T.; Ebrahimi, H.; Nourani, V. A review of the artificial intelligence methods in groundwater level modeling. *J. Hydrol.* **2019**, *572*, 336–351. [CrossRef]
8. Sattari, M.T.; Mirabbasi, R.; Sushab, R.S.; Abraham, J. Prediction of groundwater level in Ardebil plain using support vector regression and M5 tree model. *Groundwater* **2018**, *56*, 636–646. [CrossRef]
9. Zare, M.; Koch, M. Groundwater level fluctuations simulation and prediction by ANFIS-and hybrid Wavelet-ANFIS/Fuzzy C-Means (FCM) clustering models: Application to the Miandarband plain. *J. Hydro-Environ. Res.* **2018**, *18*, 63–76. [CrossRef]
10. Donnelly, J.; Abolfathi, S.; Pearson, J.; Chatrabgoun, O.; Daneshkhah, A. Gaussian process emulation of spatio-temporal outputs of a 2D inland flood model. *Water Res.* **2022**, *225*, 119100. [CrossRef]
11. Nourani, V.; Khodkar, K.; Paknezhad, N.J.; Laux, P. Deep learning-based uncertainty quantification of groundwater level predictions. *Stoch. Environ. Res. Risk Assess.* **2022**, *36*, 3081–3107. [CrossRef]
12. Zennaro, F.; Furlan, E.; Simeoni, C.; Torresan, S.; Aslan, S.; Critto, A.; Marcomini, A. Exploring machine learning potential for climate change risk assessment. *Earth-Sci. Rev.* **2021**, *220*, 103752. [CrossRef]
13. Kalu, I.; Ndehedehe, C.E.; Okwuashi, O.; Eyoh, A.E.; Ferreira, V.G. Identifying impacts of global climate teleconnection patterns on land water storage using machine learning. *J. Hydrol. Reg. Stud.* **2023**, *46*, 101346. [CrossRef]
14. Nwokolo, S.C.; Obiwulu, A.U.; Ogbulezie, J.C. Machine learning and analytical model hybridization to assess the impact of climate change on solar PV energy production. *Phys. Chem. Earth Parts A/B/C* **2023**, *130*, 103389. [CrossRef]
15. Nwokolo, S.C.; Ogbulezie, J.C.; Obiwulu, A.U. Impacts of climate change and meteo-solar parameters on photosynthetically active radiation prediction using hybrid machine learning with Physics-based models. *Adv. Space Res.* **2022**, *70*, 3614–3637. [CrossRef]
16. Jusup, M.; Holme, P.; Kanazawa, K.; Takayasu, M.; Romić, I.; Wang, Z.; Geček, S.; Lipić, T.; Podobnik, B.; Wang, L.; et al. Social physics. *Phys. Rep.* **2022**, *948*, 1–148. [CrossRef]
17. Steffen, W.; Richardson, K.; Rockström, J.; Schellnhuber, H.J.; Dube, O.P.; Dutreuil, S.; Lenton, T.M.; Lubchenco, J. The emergence and evolution of Earth System Science. *Nat. Rev. Earth Environ.* **2020**, *1*, 54–63. [CrossRef]
18. Seneviratne, S.; Nicholls, N.; Easterling, D.; Goodess, C.; Kanae, S.; Kossin, J.; Luo, Y.; Marengo, J.; McInnes, K.; Rahimi, M.; et al. Changes in Climate Extremes and Their Impacts on the Natural Physical Environment. 2012. Available online: https://library.harvard.edu/sites/default/files/static/collections/ipcc/docs/AR5_WG2_n_SREX_chapters_and_review/ii_SREX/c_Final_draft_SREX/SREX-Chap3_FINAL.pdf (accessed on 12 March 2023).
19. Wang, Z.; Jusup, M.; Guo, H.; Shi, L.; Geček, S.; Anand, M.; Perc, M.; Bauch, C.T.; Kurths, J.; Boccaletti, S.; et al. Communicating sentiment and outlook reverses inaction against collective risks. *Proc. Natl. Acad. Sci. USA* **2020**, *117*, 17650–17655. [CrossRef]
20. Gordon, J.M.; Zarmi, Y. Wind energy as a solar-driven heat engine: A thermodynamic approach. *Am. J. Phys.* **1989**, *57*, 995–998. [CrossRef]
21. Levario-Medina, S.; Valencia-Ortega, G.; Arias-Hernandez, L. Optimizacion Termodinámica de Algunas Plantas Generadoras de Energia Mediante la k-Potencia Eficiente. 2021. Available online: https://www.esfm.ipn.mx/assets/files/esfm/docs/RNAFM/articulos-2020/XXVRNAFM013.pdf (accessed on 23 April 2023).
22. Curzon, F.L.; Ahlborn, B. Efficiency of a Carnot engine at maximum power output. *Am. J. Phys.* **1975**, *43*, 22–24. [CrossRef]
23. Arias-Hernandez, L.A.; Angulo-Brown, F. A general property of endoreversible thermal engines. *J. Appl. Phys.* **1997**, *81*, 2973–2979. [CrossRef]
24. Angulo-Brown, F.; Rosales, M.A.; Barranco-Jimenez, M.A. The faint young Sun paradox: A simplified thermodynamic approach. *Adv. Astron.* **2012**, *2012*, 478957. [CrossRef]
25. Sagan, C.; Mullen, G. Earth and Mars: Evolution of atmospheres and surface temperatures. *Science* **1972**, *177*, 52–56. [CrossRef]
26. Kasting, J.F.; Grinspoon, D.H. The faint young Sun problem. In *The Sun in Time*; University of Arizona Press: Tucson, AZ, USA, 1991; pp. 447–462.
27. De Vos, A.; Flater, G. The maximum efficiency of the conversion of solar energy into wind energy. *Am. J. Phys.* **1991**, *59*, 751–754. [CrossRef]
28. De Vos, A.; Van der Wel, P. The efficiency of the conversion of solar energy into wind energy by means of Hadley cells. *Theor. Appl. Climatol.* **1993**, *46*, 193–202. [CrossRef]
29. Houghton, J. Global warming reports on progress. *Physics* **2005**, *68*, 1340–1403.
30. Wang, R.; Li, L.; Gentine, P.; Zhang, Y.; Chen, J.; Chen, X.; Chen, L.; Ning, L.; Yuan, L.; Lü, G. Recent increase in the observation-derived land evapotranspiration due to global warming. *Environ. Res. Lett.* **2022**, *17*, 024020. [CrossRef]
31. Chi, J.; Kim, H.c. Prediction of arctic sea ice concentration using a fully data driven deep neural network. *Remote Sens.* **2017**, *9*, 1305. [CrossRef]
32. Asthana, T.; Krim, H.; Sun, X.; Roheda, S.; Xie, L. Atlantic hurricane activity prediction: A machine learning approach. *Atmosphere* **2021**, *12*, 455. [CrossRef]
33. Nieves, V.; Radin, C.; Camps-Valls, G. Predicting regional coastal sea level changes with machine learning. *Sci. Rep.* **2021**, *11*, 7650. [CrossRef]
34. Khasnis, A.A.; Nettleman, M.D. Global warming and infectious disease. *Arch. Med. Res.* **2005**, *36*, 689–696. [CrossRef] [PubMed]
35. Sidhu, B.S.; Mehrabi, Z.; Ramankutty, N.; Kandlikar, M. How can machine learning help in understanding the impact of climate change on crop yields? *Environ. Res. Lett.* **2023**, *18*, 024008. [CrossRef]
36. Zheng, H. Analysis of global warming using machine learning. *Comput. Water Energy Environ. Eng.* **2018**, *7*, 127. [CrossRef]

37. Cheremisin, G.; Egorov, D.; Kravchenko, O.; Dev, A. Deep convolutional neural network for reconstructing the cloud phase distribution from level-1b MODIS data. *Proc. AIP Conf. Proc.* **2023**, *2819*, 030005.
38. Miloshevich, G.; Cozian, B.; Abry, P.; Borgnat, P.; Bouchet, F. Probabilistic forecasts of extreme heatwaves using convolutional neural networks in a regime of lack of data. *Phys. Rev. Fluids* **2023**, *8*, 040501. [CrossRef]
39. Farhangmehr, V.; Cobo, J.H.; Mohammadian, A.; Payeur, P.; Shirkhani, H.; Imanian, H. A Convolutional Neural Network Model for Soil Temperature Prediction under Ordinary and Hot Weather Conditions: Comparison with a Multilayer Perceptron Model. *Sustainability* **2023**, *15*, 7897. [CrossRef]
40. Hassan, K.M.A. Predicting Future Global Sea Level Rise From Climate Change Variables Using Deep Learnin. *Int. J. Comput. Digit. Syst.* **2023**. [CrossRef]
41. Ghimire, S.; Nguyen-Huy, T.; Prasad, R.; Deo, R.C.; Casillas-Perez, D.; Salcedo-Sanz, S.; Bhandari, B. Hybrid convolutional neural network-multilayer perceptron model for solar radiation prediction. *Cogn. Comput.* **2023**, *15*, 645–671. [CrossRef]
42. Larson, A.; Hendawi, A.; Boving, T.; Pradhanang, S.M.; Akanda, A.S. Discerning Watershed Response to Hydroclimatic Extremes with a Deep Convolutional Residual Regressive Neural Network. *Hydrology* **2023**, *10*, 116. [CrossRef]
43. Jonnalagadda, J.; Hashemi, M. Long Lead ENSO Forecast Using an Adaptive Graph Convolutional Recurrent Neural Network. *Eng. Proc.* **2023**, *39*, 5.
44. Lacombe, R.; Grossman, H.; Hendren, L.; Lüdeke, D. Improving extreme weather events detection with light-weight neural networks. *arXiv* **2023**, arXiv:2304.00176.
45. Raman, R.; Mewada, B.; Meenakshi, R.; Jayaseelan, G.; Sharmila, K.S.; Taqui, S.N.; Al-Ammar, E.A.; Wabaidur, S.M.; Iqbal, A. Forecasting the PV Power Utilizing a Combined Convolutional Neural Network and Long Short-Term Memory Model. *Electr. Power Components Syst.* **2023**, 1–17. [CrossRef]
46. Lin, F.; Zhang, Y.; Wang, J. Recent advances in intra-hour solar forecasting: A review of ground-based sky image methods. *Int. J. Forecast.* **2023**, *39*, 244–265. [CrossRef]
47. Caldas, M.; Alonso-Suárez, R. Very short-term solar irradiance forecast using all-sky imaging and real-time irradiance measurements. *Renew. Energy* **2019**, *143*, 1643–1658. [CrossRef]
48. Pedro, H.T.; Coimbra, C.F.; David, M.; Lauret, P. Assessment of machine learning techniques for deterministic and probabilistic intra-hour solar forecasts. *Renew. Energy* **2018**, *123*, 191–203. [CrossRef]
49. Kamadinata, J.O.; Ken, T.L.; Suwa, T. Sky image-based solar irradiance prediction methodologies using artificial neural networks. *Renew. Energy* **2019**, *134*, 837–845. [CrossRef]
50. Barranco-Jimenez, M.A.; Chimal-Eguia, J.C.; Angulo-Brown, F. The Gordon and Zarmi model for convective atmospheric cells under the ecological criterion applied to the planets of the solar system. *Rev. Mex. Fis.* **2006**, *52*, 205–212.
51. Ocampo-Garcia, A. Optimizacion Termodinamica y Termoeconomica de Modelos Extendidos de Maquinas Endorreversibles. Ph.D. Thesis, Instituto Politecnico Nacional, Mexico City, Mexico, 2020.
52. Angulo-Brown, F.; Arias-Hernandez, L.A.; Santillan, M. On some connections between first order irreversible thermodynamics and finite-time thermodynamics. *Rev. Mex. Fis.* **2002**, *48*, 182–192.
53. Norma Sanchez, F.; Angulo-Brown, M.B.J. Posibles futuros escenarios de la temperatura superficial de la Tierra con la evolucion de la constante solar. In Proceedings of the XXII Congreso Nacional de Termodinamica, Sociedad Mexicana de Termodinamica A.C., Mexico City, Mexico, 10–12 September 2007.
54. Barranco-Jimenez, M.A.; Angulo-Brown, F. A simple model on the influence of the greenhouse effect on the efficiency of solar-to-wind energy conversion. *Il Nuovo Cimento C* **2003**, *26*, 535–552.
55. Barranco-Jimenez, M.A.; Angulo-Brown, F. A nonendoreversible model for wind energy as a solar-driven heat engine. *J. Appl. Phys.* **1996**, *80*, 4872–4876. [CrossRef]
56. National Oceanic and Atmospheric Administration. Trends in Atmospheric Carbon Dioxide. 2023. Available online: https://gml.noaa.gov/ccgg/trends/ (accessed on 3 July 2023).
57. Berkeley Earth. Global Warming Data Overview. 2023. Available online: https://berkeleyearth.org/data/ (accessed on 3 July 2023).
58. National Center for Atmosferic Research. Global Surface Temperatures: BEST: Berkeley Earth Surface Temperatures. 2023. Available online: https://climatedataguide.ucar.edu/climate-data/global-surface-temperatures-best-berkeley-earth-surface-temperatures (accessed on 3 June 2023).
59. National Aeronautics and Space Administration. GISS Surface Temperature Analysis (GISTEMP v4). 2023. Available online: https://data.giss.nasa.gov/gistemp/ (accessed on 3 June 2023).
60. Pierrehumbert, R.T. Infrared radiation and planetary temperature. *Phys. Today* **2011**, *64*, 33–38. [CrossRef]
61. Curry, J.A.; Webster, P.J. *Thermodynamics of Atmospheres and Oceans*; Elsevier: Amsterdam, The Netherlands, 1998.
62. von Paris, P.; Rauer, H.; Grenfell, J.L.; Patzer, B.; Hedelt, P.; Stracke, B.; Trautmann, T.; Schreier, F. Warming the early Earth—CO2 reconsidered. *Planet. Space Sci.* **2008**, *56*, 1244–1259. [CrossRef]
63. Krasnopolsky, V.M.; Fox-Rabinovitz, M.S. Complex hybrid models combining deterministic and machine learning components for numerical climate modeling and weather prediction. *Neural Netw.* **2006**, *19*, 122–134. [CrossRef] [PubMed]
64. Schmidt, G.A.; Sherwood, S. A practical philosophy of complex climate modelling. *Eur. J. Philos. Sci.* **2015**, *5*, 149–169. [CrossRef]
65. Knutti, R.; Rugenstein, M.A. Feedbacks, climate sensitivity and the limits of linear models. *Philos. Trans. R. Soc. A Math. Phys. Eng. Sci.* **2015**, *373*, 20150146. [CrossRef] [PubMed]

66. Visconti, G. *Fundamentals of Physics and Chemistry of the Atmosphere*; Springer: Berlin/Heidelberg, Germany, 2001.
67. North, G.R.; Cahalan, R.F.; Coakley, J.A., Jr. Energy balance climate models. *Rev. Geophys.* **1981**, *19*, 91–121. [CrossRef]
68. Levario Medina, S. Estudio de Algunas Funciones Compromiso y Sus Efectos en la Optimización Termodinámica en los Modelos de Convertidores de Energía. Ph.D. Thesis, Escuela Superior de Física y Matemáticas, Instituto Politécnico Nacional, Mexico City, Mexico, 2021.